Influence of the different capacitor configurations of the supply system on the efficiency of the rail accelerator

PAWEŁ PIEKIELNY [ID]**, ANDRZEJ WAINDOK** [ID][✉]**, PAWEŁ MAMALA** [ID]

Department of Electrical Engineering and Mechatronics, Opole University of Technology
Prószkowska 76 str., 45-758 Opole, Poland

e-mail: {p.piekielny/✉ a.waindok}@po.edu.pl, mamalap@gmail.com

Abstract: The influence of the capacitor configuration in the pulse supply system for rail accelerators on its efficiency was investigated in the paper. Two different configurations were compared: the first with a parallel connection of capacitors and the second with a parallel-series connection. In both cases, the same number of capacitors was assumed. All other parameters of the device were kept constant, i.e. mass and dimensions of the armature, rail length and stator geometry. A field-circuit model was used to analyse numerically the transients for different capacitor configurations and voltage values. The model was verified experimentally.

Key words: capacitor pulse supply system, electrodynamic accelerators, transient calculations

1. Introduction

The interest in rail accelerators is increasing, especially in military applications [1–3]. However, there is also an increasing interest observed in other applications, e.g. geological research (impact measurements) or measuring of impact resistance of materials (for space shuttle covers, satellites and aeroplanes) [4–6]. There are also articles proposing using the electromagnetic gun principle for transport [7].

Conventional gas systems for impact testing do not achieve the required energy and synchronisation parameters due to using gas to drive the impact member. The electro-magnetic gun overcomes these limitations as it allows precise control of the parameters of the armature [8–11]. The problem is in the costs. Although it is relatively low for the accelerator itself, the power supply system, including control and monitoring systems, could be costly. Thus, investigations are carried out to increase the system's efficiency. One possibility is to increase the magnetic flux in the armature volume [12].

Advanced numerical techniques, such as the Finite Element Method (FEM) and Finite Difference Method (FDM), are widely used to simulate the flow of electromagnetic fields and analyse the impact of changes on the performance of accelerators, transformers, and magnetic bearings. These techniques enable engineers to predict the behaviour of electromagnetic fields in various configurations, which is crucial in designing and optimising these devices. For accelerators, numerical simulations enable the analysis of electric and magnetic fields to design optimal magnetic systems, optimise particle trajectories, and evaluate the influence of electromagnetic field disturbances on beam stability. By utilising advanced numerical techniques, engineers can conduct virtual tests and analyses, speeding up the design process, minimising the risk of costly errors, and optimising the energy efficiency and performance of electromagnetic devices [13–15]. Increasing efficiency can be achieved by optimising the rail design, propulsion system, and railgun configuration. Optimal rail shapes and materials, an efficient propulsion system, and proper alignment and geometry of components can reduce energy losses, enhance energy transfer efficiency, and improve the overall effectiveness of the railgun [16, 17]. Another one is changing the supply system. Rail accelerators use the electromagnetic phenomenon to accelerate objects by passing a current through conducting material rails, generating an electromagnetic force. Thanks to advancements in electronics and materials science, many efficient power sources for rail accelerators were developed, which can be divided into inductive, rotational, and capacitive [18]. As an essential element of the power system, there is also the way the energy is delivered, which can be divided into two main categories: the first releases all the energy at the same time, while the second allows the energy to be divided into several smaller pulses [19]. An example of an inductive power supply is the XRAM generator, which uses inductive coils to multiply current by charging them and then quickly switching [20]. Another solution is the compulsator, which uses rotational momentum to store kinetic energy and then transfer it as a current pulse [21]. The final method for powering rail accelerators is to use capacitive power sources based on capacitors [10]. Capacitors can serve as a storage for electrical energy, which can then be transferred to the rail accelerator as current pulses. In the presented work, the supply system based on capacitors was used, and two different connections were analysed. The connection influences the current waveforms (pulse duration and amplitude), directly affecting the accelerator performance.

2. Field-circuit numerical model

For the analysis of the efficiency, the previously verified field-circuit model was used [12, 14, 15], which block diagram is shown in Fig. 1. The field calculations were performed in the ANSYS Maxwell magnetostatics module, which uses the reduced magnetic scalar potential ϕ. For air and rails, the following equation is calculated:

$$\nabla \cdot (\mu_0 \nabla \phi) = -\nabla \cdot \left(\mu_0 \vec{H}_P \right), \tag{1}$$

where $\vec{H}_P$ is the magnetic field intensity vector calculated using the Biot–Savart law.

In a ferromagnetic region, for which the current density $\vec{J}_s = 0$, the homogeneous partial differential equation for the scalar potential is solved:

$$\nabla \cdot (\mu_0 \nabla \phi) = 0. \tag{2}$$

The magnetic flux passing through the surface S (bounded by the armature and rails) is determined as the integral of the scalar product of the magnetic flux density vector and the unit normal vector, over the closed surface of this circuit:

$$\Phi_S = \int_S \vec{B} \cdot \vec{n} \, \mathrm{d}S, \tag{3}$$

where: Φ_S is the flux limited by the area S; $\vec{B}$ is the magnetic flux density vector; $\vec{n}$ is the unit vector normal to the surface S.

The Lorentz force F_z acting on the armature in the exit direction was calculated from the relationship:

$$F_z = \int_\Omega mN^T \left(J \times B \right) \mathrm{d}\Omega_m, \tag{4}$$

where Ω_m is the armature volume [m^3] and N^T is the shape function vector.

The dynamic inductance L_d, which is an essential parameter in the field-circuit model, was calculated as the partial derivative of the flux Φ_S associated with the rails in relation to the current:

$$L_d = \frac{\partial \Phi_S}{\partial i}. \tag{5}$$

The circuit model is described by a system of three equations describing the motion of the armature and the current intensity waveform:

$$\frac{\mathrm{d}v}{\mathrm{d}t} = \frac{F\left(i, z \right) - Dv - D_p v^2}{m}, \tag{6}$$

$$\frac{\mathrm{d}z}{\mathrm{d}t} = v, \tag{7}$$

$$\frac{\mathrm{d}i}{\mathrm{d}t} = \frac{-Ri - \dfrac{\mathrm{d}}{\mathrm{d}z}\left(\Phi_s \left(i, z \right) \right) v - \dfrac{q}{C}}{L_d \left(i, z \right)}, \tag{8}$$

where: z is the armature position, v is the armature velocity, m is the armature mass, D is the kinetic friction coefficient, D_p is the air friction coefficient, R is the circuit resistance, q is the charge, i is the excitation current, C is the capacitance, $F(i, z)$ is the force, $\Phi_s(i, z)$ is the magnetic flux, $L_d(i, z)$ is the dynamic inductance.

Equations (6) and (7) describe the mechanical part of the model, while Eq. (8) describes the electrical domain. In Eq. (8) in nominator, the voltage drop on the resistance, the electromotive force and capacitor voltage are included. In the denominator, due to the nonlinear $B(H)$ curve of the iron core, the dynamic inductance is used. The values of magnetic flux, electrodynamic force, and dynamic inductance were calculated using the FEM. The permanent magnet field was determined using its demagnetisation curve.

Parameters such as resistance (R) and inductance (L) values depend on the position of the driven member (projectile). The inductance value depends additionally on the excitation current value, which is due to the core's nonlinear $B(H)$ curve. The power source parameters were assumed to be independent of the current value and projectile position. Despite the simplifications used, it was noted that they slightly affected the final result. The implementation of the field-circuit model in MATLAB/Simulink software is shown in Fig. 2.

The capacitor bank was divided into three sections (symmetrical in terms of capacity), which were triggered simultaneously from separate thyristor keys. This configuration was similar to the physical one used for extended measurement verification. The total power capacity assumed for initial calculations is 300 mF for a parallel connection and 75 mF for a series-parallel connection. In order to maintain a constant energy accumulated in the supply system, the starting voltage of the shot for the series-parallel connection system was twice as high as for the parallel one. The comparative parameter was the calculated muzzle velocity and efficiency of the whole system (accelerator + supply system) [22].
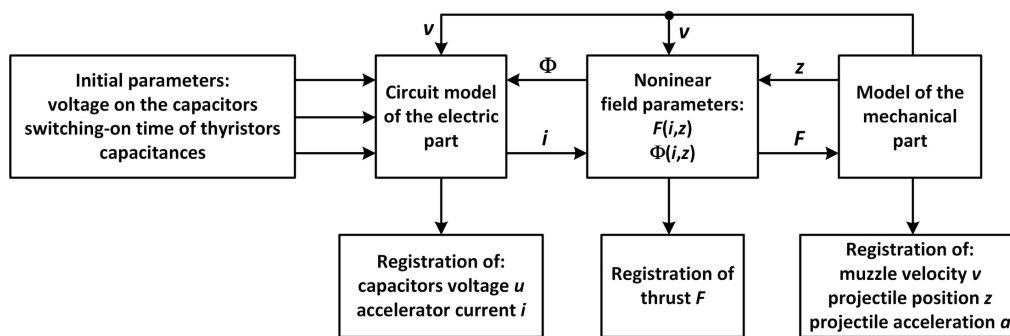
Fig. 1. Block diagram of the field-circuit model [12]
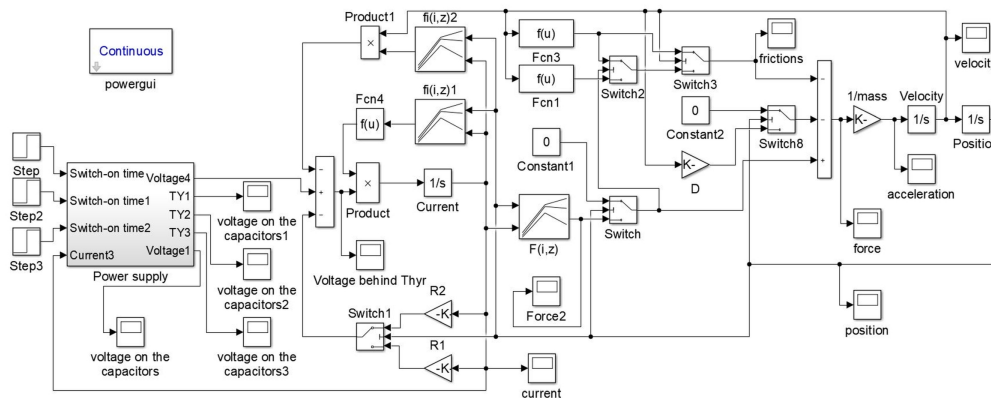
Fig. 2. Field-circuit model in Simulink software

3. Physical model

For the rail accelerator, a construction with permanent magnets was used (PMRA – permanent magnet rail accelerator), which is presented in Fig. 3. This type of accelerator was chosen due to increased performance for lower current values compared to iron-less or iron-core accelerators. The length of the core is 200 mm, the length of the rails is 300 mm, the rails cross-section is 85.8 mm^2, and the width and height of the accelerator is 84 × 60 mm. For the permanent magnet,

a NdFeB45 material was used. The detailed physical parameters are given in [22]. The capacitor connections are presented in Fig. 4. The picture and electric scheme of the whole experimental setup are shown in Fig. 5. For the capacitor charging, the 3-phase autotransformer with a rectifier was used. All three sections are charged parallel. Current and voltage waveforms were acquired using a Tektronix MSO44 4-BW-500 oscilloscope. For current wave measurement, the Rogowski coil was used. The muzzle velocity, which is an important parameter for efficiency determination, was measured using the chronograph.
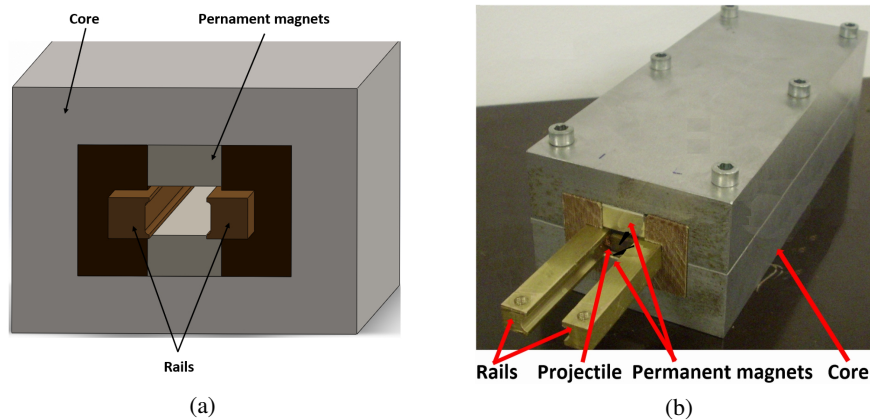
Fig. 3. The outlines (a) and pictures (b) of PMRA
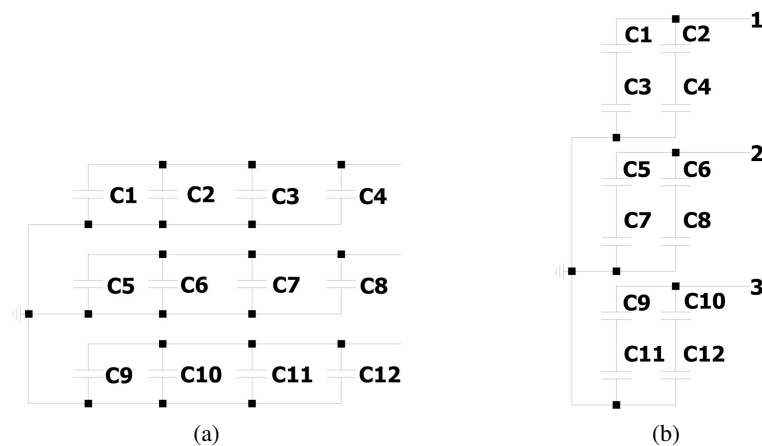
Fig. 4. Parallel (a) and parallel-series (b) connection of capacitors

The parameters assumed in the circuit model are given in Table 1. The mechanical parameters are the same both in parallel and parallel-series connections. The electrical parameters differ in both cases, i.e. the resistance of the power supply is higher in the case of the parallel-series connection, while the inductance is slightly lower.
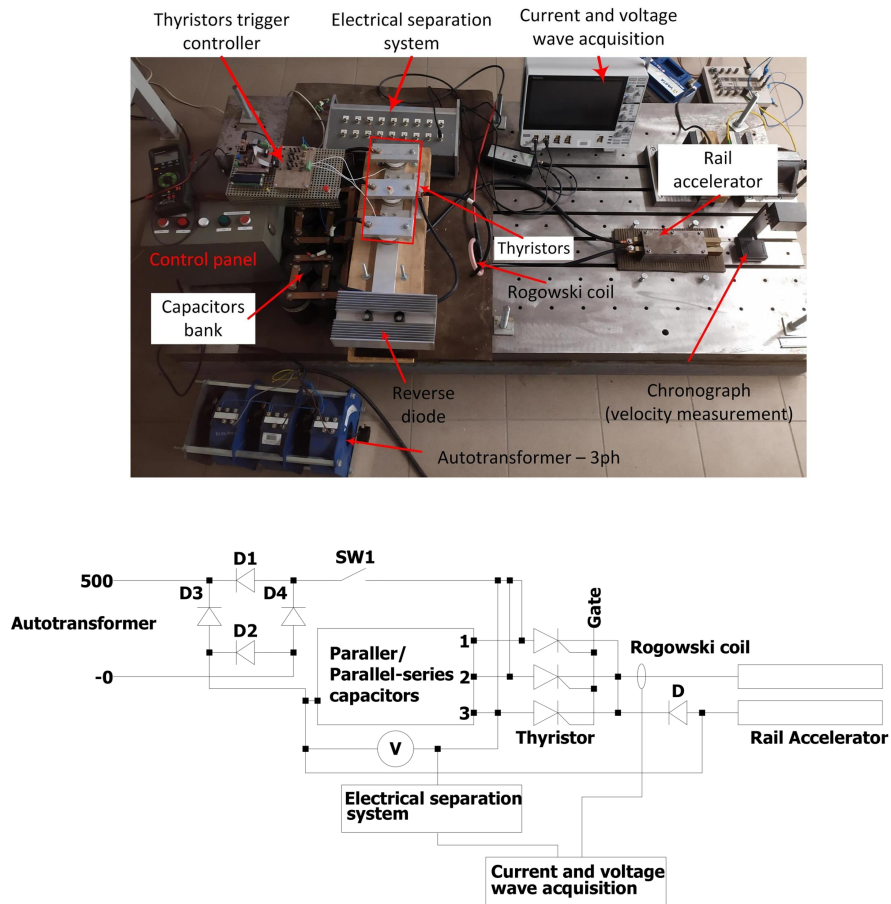
Fig. 5. Picture and electrical circuit diagram of the experimental setup

Table 1. Main circuit parameters (determined experimentally)

Quantity	Unit	Value (parallel)	Value (parallel-series)
Projectile mass m	[g]	5.13	5.13
Friction coefficient D	[Ns/m]	0.2	0.2
Drag coefficient C_x	–	1.05	1.05
Resistance of the power supply circuit R	[mΩ]	2.1	3.5
Inductance of the power supply circuit L	[μH]	1.75	1.52
Capacity of the capacitor bank	[F]	0.132	0.033

4. Research results

4.1. Preliminary calculation results

The preliminary analysis was conducted for four input energy values (Table 2) keeping the supply parameters constant (R = 1.8 μΩ, L = 0.94 μH). For lower energy values (1.5 kJ and 6 kJ), the more effective connection is a parallel one. For higher energy values, the more effective system is a series-parallel connection. From Fig. 6, it is visible that both connection configurations give the same result for approximately E = 10 kJ. In the range from 1.5 kJ to 12 kJ there is only a slight difference between two analysed connections visible. For higher input energy values, the parallel-series connection is more effective (allows one to reach higher muzzle velocity).

Table 2. Initial calculation results

Connection arrangement	C [mF]	U [V]	E [kJ]	v_{cal} [m/s]	η [%]
parallel	300	100	1.5	86.89	1.82
parallel-series	75	200	1.5	75.61	1.40
parallel	300	200	6.0	248.7	3.72
parallel-series	75	400	6.0	233.8	3.34
parallel	300	300	13.5	404.0	4.47
parallel-series	75	600	13.5	421.4	4.81
parallel	300	400	24.0	539.9	4.86
parallel-series	75	800	24.0	610.4	5.67
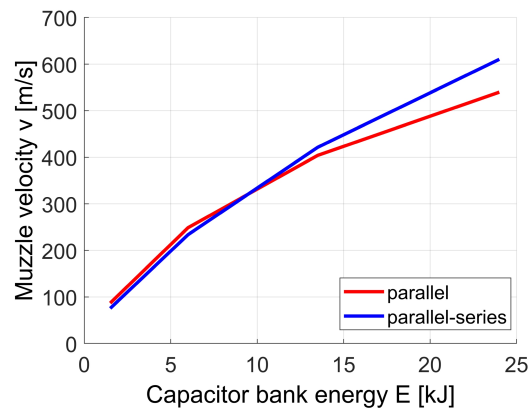
Fig. 6. Calculated muzzle velocity vs. capacitor bank energy

In Fig. 7, the current waves for two cases from Table 2 are presented, i.e. the lowest and highest energy values. For the parallel connection of capacitors, the current pulse has a longer duration and a smaller maximum value compared to the parallel-series connection. It is due to higher

capacitance and lower voltage value. In Fig. 7(b), the time of leaving the rails is visible as the abrupt current value decreases.
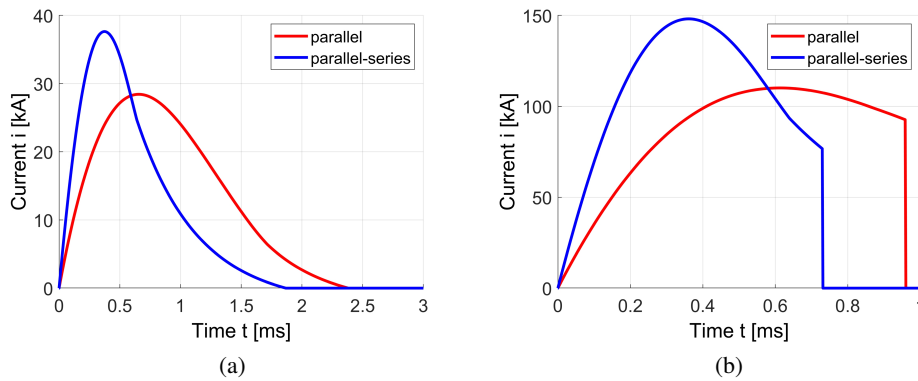
Fig. 7. Calculation results for excitation current vs time: (a) 100 V/200 V; (b) 400 V/800 V

As the amplitude of the current increases, the thrust value increases, as well. Thus, acceleration increases and the discharge velocity can be higher. Based on preliminary calculations, the velocity and heading characteristics were determined (Fig. 8). Due to its higher voltage and maximum current value, the parallel-series connection achieves a higher efficiency for higher energy values than the parallel connection (as in the case of exit velocity).
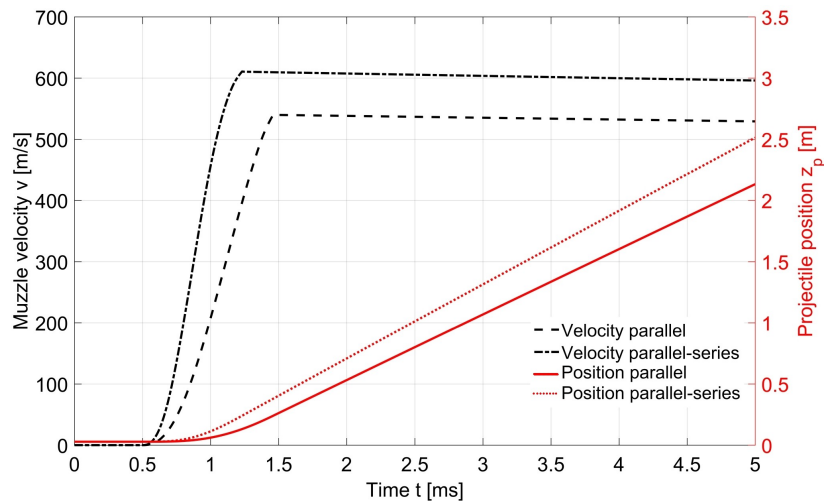
Fig. 8. Calculated projectile velocity and position for 400 V/800 V

4.2. Transient calculations and measurement results

In Fig. 9, the measurement results of a current wave for two different configurations under the same energy are shown. In the calculation models, the paramters of the circuits given in Table 1 were assumed. To keep the same energy in the capacitor, the voltage for the parallel-series connection was twice as high as for the parallel one. Despite this, the maximum current value is only about 10% higher in the case of the parallel-series connection. The duration of the current pulse is 50% higher in the case of the parallel connection and does not depend on the supply voltage value.

(a)

(b)

(c)
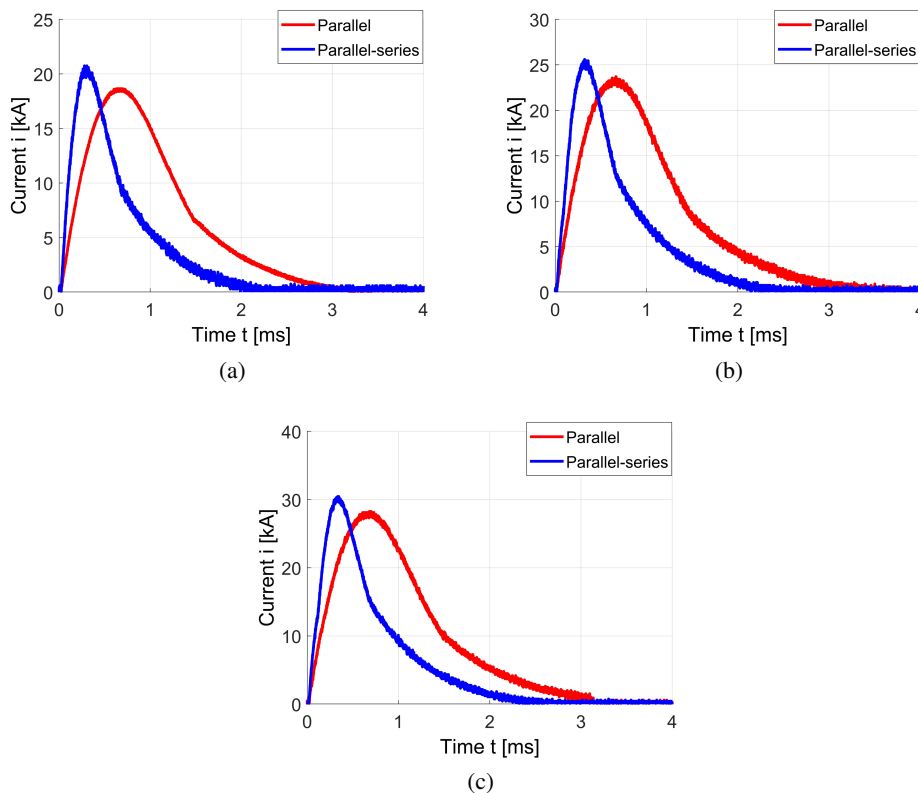
Fig. 9. Excitation current vs. time: (a) 103 V/199 V; (b) 128 V/250 V; (c) 155 V/299 V

The examination of the field-circuit model was carried out, as well. The results for both capacitor configurations are presented in Figs. 10 and 11. In the case of the parallel configuration (Fig. 10), for lower investigated voltage values (103 V and 128 V), there is a very good conformity visible between the field-circuit model and experimental results. For higher voltage values (155 V and 181 V), the slope of the current wave is almost the same, but there are some differences visible in the signal duration. In the experimental results, the current decreases to zero latterly compared to the calculations (Figs. 10(c) and 10(d)). It is due to some simplification of the mechanical part of the model. Some parameters, like friction forces, were assumed to be linear, but they could change vs. velocity or temperature, which was not investigated in the paper.
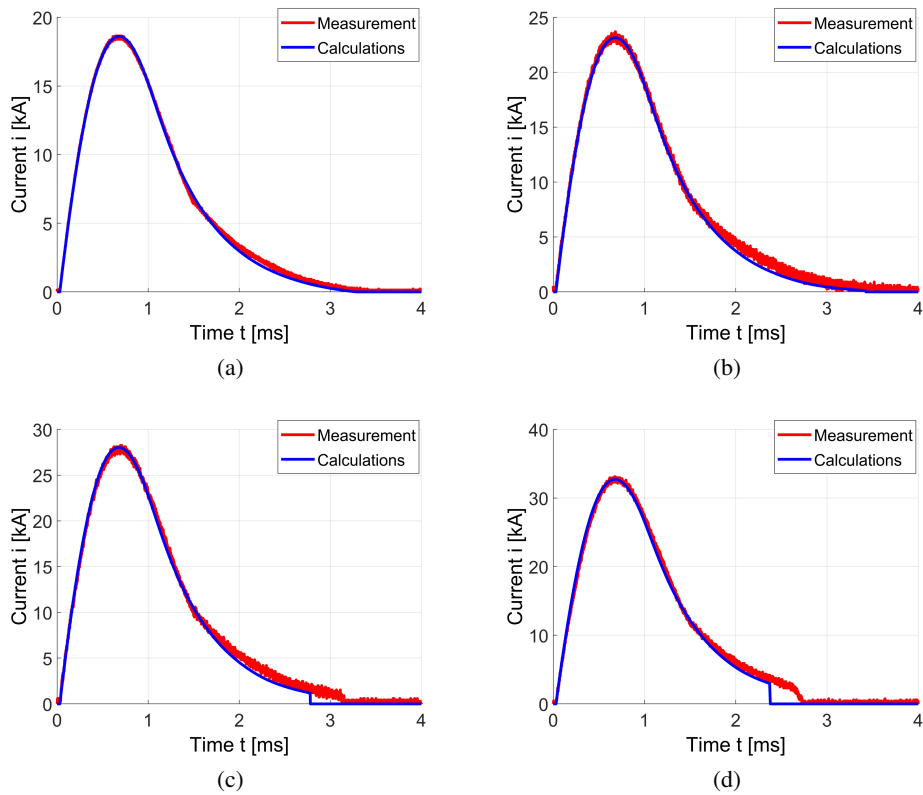
Fig. 10. Measurement verification of field-circuit model for parallel connection of capacitors:
(a) $U = 103$ V; (b) $U = 128$ V; (c) $U = 155$ V; (d) $U = 181$ V

In the case of the parallel-series connection (higher voltages) more significant differences between measurements and calculations are observed (Fig. 11). The shape of the excitation current is the same in tests and model up to the moment, where the reverse diode starts to work. At that moment, the slope of the current differs in measurements and calculations. In the case of lower voltage (199 V) it is only slightly visible, while along with the increasing of the capacitor voltage, the discrepancy also increases (Figs. 11(b), 11(c) and 11(d)). It could be due to the simplified reverse diode model. Considering extreme working conditions, the model, although imperfect, allows for the prediction of the current waves.

The most important parameter of the rail accelerator is the muzzle velocity. Due to different physical phenomena occurring in the PMRA construction, it was essential to verify experimentally the mathematical model, which is an approximation of reality, for the muzzle velocity. The results are presented in Table 3. The differences in the case of the parallel connection are less than 14% (for lower voltage) and decrease with the voltage increasing (for 175 V there is only 4.5% error). In the case of the parallel-series connection, the differences are higher and are within the limit of $6\% \div 25\%$.
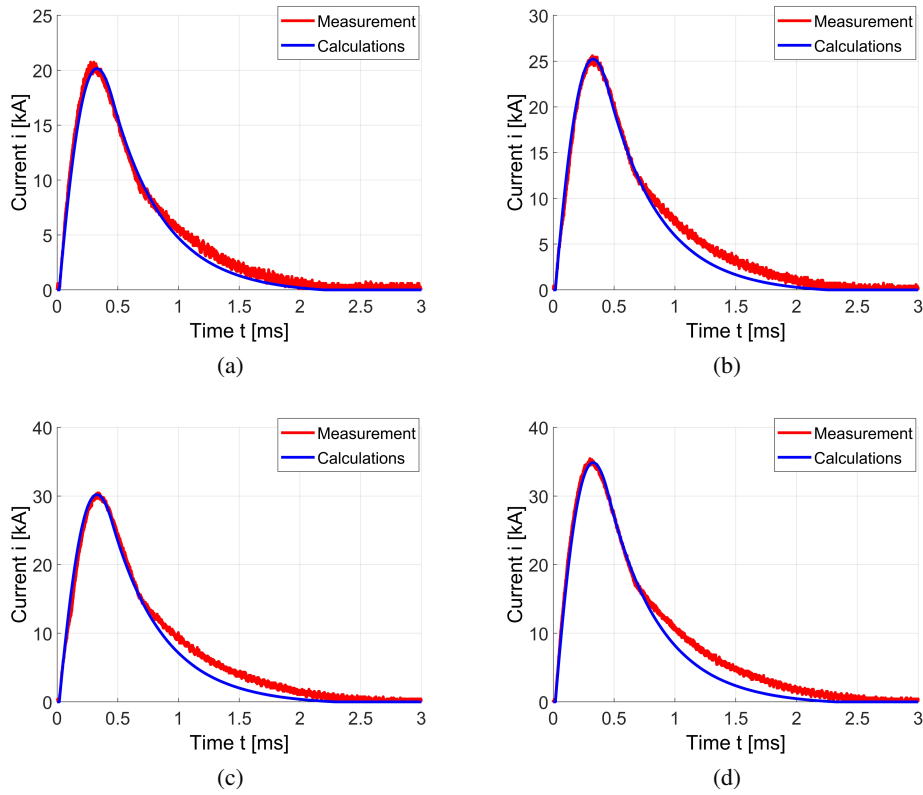
Fig. 11. Measurement verification of field-circuit model for parallel-series connection of capacitors: (a) $U = 199$ V; (b) $U = 250$ V; (c) $U = 299$ V; (d) $U = 344$ V

Both in measurement and calculation results, the velocity is higher for the parallel connection of capacitors (for the same input energy). Due to experimental difficulties, for higher capacitor energy values (above approx. 2 kJ), only the calculations were made, which results are presented in Fig. 12.

Some additional comment is needed according to the shape of the discharge current wave. The analytical expression (simplified one, without taking into account armature movement and nonlinearities) describing the transients of the RLC circuit depends on the dumping factor $\xi = R/2\sqrt{C/L}$. In the analysed cases of capacitor configurations $\xi < 1$, which means, that it is an underdamped case. Thus, the current wave is expressed in the following form:

$$i\left(t\right) = \frac{U_0}{\omega L} e^{-\frac{Rt}{2L}} \sin\left(\omega t\right), \tag{9}$$

where: U_0 is the initial capacitor voltage, R is the circuit resistance, L is the circuit inductance, ω is the dumped angular frequency.

Table 3. Measurement verification of muzzle velocity

Voltage	Capacitor energy	Parallel connection		Parallel-series connection	
U[V]	E [J]	v_{mes} [m/s]	v_{cal} [m/s]	v_{mes} [m/s]	v_{cal} [m/s]
70/140	323.4	37.4	32.20	20.4	15.81
100/200	660.0	61.9	59.53	37.6	31.98
125/250	1031.25	86.4	84.11	50.9	47.78
150/300	1485.0	110.8	112.60	71.5	64.85
175/350	2021.25	135.1	141.67	91.3	82.05
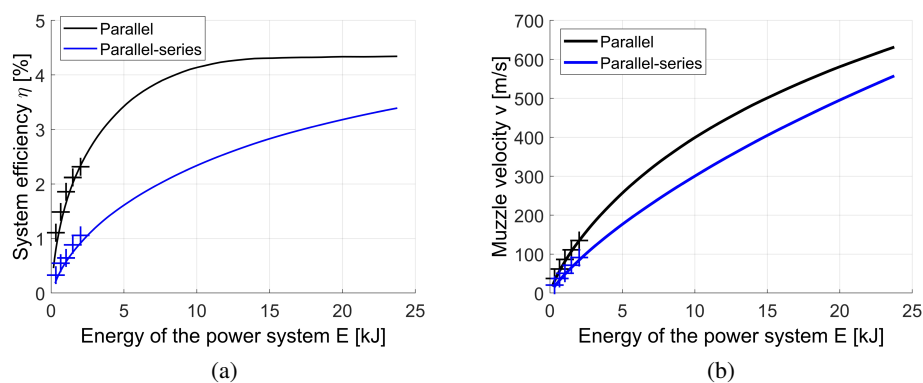
Fig. 12. (a) System efficiency vs. energy of the power system ("+" measurements); (b) muzzle velocity vs. energy of the power system ("+" measurements)

The dumped angular frequency is determined from the following expression:

$$\omega = \sqrt{\left(\frac{1}{LC}\right)^2 - \left(\frac{R}{2L}\right)^2}. \tag{10}$$

To maintain constant power supply energy for the analysed connection systems, the U_0 value is twice as high in the case of the parallel-series connection and the C value is four times lower compared to the parallel connection. Additionally, in the parallel-series connection, the R-value is 66% higher and inductance 15% lower than in the parallel connection (the values were determined experimentally). Thus, the connection of capacitors significantly influences the shape of the current pulse waveform in terms of the maximum value and the pulse duration. The lower current rising

time for the parallel connection results from

$$\underbrace{\sqrt{\left(\frac{1}{0.87 \cdot L \cdot 0.25 \cdot C}\right)^2 - \left(\frac{1.66 \cdot R}{2 \cdot 0.87 \cdot L}\right)^2}}_{\omega_{\text{peak(parallel-series)}}} > \underbrace{\sqrt{\left(\frac{1}{LC}\right)^2 - \left(\frac{R}{2L}\right)^2}}_{\omega_{\text{peak(parallel)}}}$$

$$(4316 \text{ rad/s} > 1991 \text{ rad/s}). \tag{11}$$

Thus, the calculated rising time of the current for the parallel connection is equal to $t_1 = 0.79$ ms and for the parallel-series connection to $t_2 = 0.36$ ms. Both values are similar to the measured ones.

The higher maximum current value for the parallel-series connection results from

$$\underbrace{\frac{2U_0}{1.89\omega L}e^{-\frac{1.66 \cdot Rt_1}{2 \cdot 0.87 \cdot L}}}_{I_{\text{peak(parallel-series)}}} > \underbrace{\frac{U_0}{\omega L}e^{-\frac{Rt_2}{2L}}}_{I_{\text{peak(parallel)}}}. \tag{12}$$

Substituting $U_0 = 100$ V, we obtain the peak values of currents: $I_{\text{peak}} = 18.4$ kA for the parallel connection and $I_{\text{peak}} = 20$ kA for the parallel-series connection, which corresponds to the measured values. It should be mentioned that after discharging the capacitor, the circuit changes into RL one (the current flows through the protection diode).

The efficiency value increases vs energy (Fig. 12(a)), however, in the case of the parallel connection, the saturation effect is observed ($\eta_{\text{max}} = 4.3\%$). The discrepancy between the parallel and parallel-series connection decreases vs. energy. Although, even for energies above 20 kJ, the efficiency is still better for the parallel connection (4.3% vs. 3.4%). It is due to the lower resistance of the parallel capacitor connection and shorter current pulse duration in the parallel-series connection. It could be also explained by using the action integral. By simplifying the problem (i.e. omitting nonlinearities and dissipation energy), the inductive energy is proportional to squared current $\sim i^2$. Calculating the action integral for this parameter over time in both parallel and parallel-series connections, we obtain that it is much higher (more than 50%) in the case of the parallel connection. It means, that more energy is transferred from the source to the rails for the parallel capacitor connection, and thus, the efficiency increases.

The muzzle velocity reflects the efficiency curve (Fig. 12(b)). Along with the increasing of supply voltage, the velocity increases. The slope of the curve is similar in both parallel and parallel-series connections. The value of the muzzle velocity is higher in the case of the parallel connection. It should be emphasised that the phenomena associated with supersonic speeds were not considered in the presented model. It means the calculated muzzle velocity curves for higher energy values could differ from the real one.

5. Conclusions

Based on the investigation, the following conclusion could be formulated:
- For the investigated permanent magnet rail accelerator, higher efficiency of the system and higher muzzle velocity are observed for the parallel connection of capacitors.

- The better results for the parallel connection, compared to the parallel-series one, are due to the higher action integral. It means, that the energy transferred to the accelerator is higher in the case of the parallel connection.
- The selection of the capacitor connection should take into account the distance along which the projectile is accelerated while taking into account the energy of the power supply system.
- It is recommended to optimise the capacitor connection and the power supply system to achieve even higher efficiency and muzzle velocity.

The presented numerical model was verified experimentally for voltages up to 175/350 V. Thus, the extrapolation for higher voltage value could be only an approximation of the real object. Despite this, the developed model can be used for the initial approximate prediction of the parameters of the rail accelerator.

References

[1] Hundertmark S., Lancelle D., *A scenario for a future European shipboard railgun*, IEEE Transactions on Plasma Science, vol. 43, no. 5, pp. 1194–1197 (2015), DOI: 10.1109/TPS.2015.2403863.

[2] Gallant J., Vancaeyzeele T., Lauwens B., Wild B., Alouahabi F., Schneider M., *Design considerations for an electromagnetic railgun firing intelligent bursts to be used against antiship missiles*, IEEE Transactions on Plasma Science, vol. 43, no. 5, pp. 1179–1184 (2015), DOI: 10.1109/TPS.2015.2416774.

[3] Lehmann P., Reck B., Vo M.D., Behrens J., *Acceleration of a suborbital payload using an electromagnetic railgun*, IEEE Trans. Magn., vol. 43, no. 1, pp. 480–485 (2007), DOI: 10.1109/TMAG.2006.887666.

[4] Gores P.A., Vincent G., Schneider M., Spray J.G., *Appraisal of Rapid-Fire Electromagnetic Launch Effects on Ceramic Targets*, IEEE Transactions on Plasma Science, vol. 47, no. 8, pp. 4175–4180 (2019), DOI: 10.1109/TPS.2019.2921731.

[5] Vricella A., Delfini A., Pacciani A., Pastore R., Micheli D., Rubini G., Marchetti M., Santoni F., *A new advanced railgun system for debris impact study*, in Procedia Structural Integrity, Elsevier B.V., pp. 545–552 (2017). DOI: 10.1016/j.prostr.2017.04.044.

[6] Slimane S.A., Slimane A., Ahmed G., Boudjemai A., Said K., Amine S., Mouloud D., *Hypervelocity impact on honeycomb structure reinforced with bi-layer ceramic/aluminum facesheets used for spacecraft shielding*, Mechanics of Advanced Materials and Structures, vol. 29, no. 25, pp. 4487–4505 (2022), DOI: 10.1080/15376494.2021.1931991.

[7] Siemenn A.E. Deo B., Ng F., Zhou J., Owens C., Atue S.U., Forsuelo M., *A Railgun Secondary Propulsion System for High-Speed Hyperloop Transportation*, IEEE Transactions on Plasma Science, vol. 51, no. 1, pp. 243–248 (2023), DOI: 10.1109/TPS.2022.3232406.

[8] Schneider M., Vincent G., Hogan J.D., Spray J.G., *The use of a railgun facility for dynamic fracture of brittle materials*, IEEE Transactions on Plasma Science, vol. 43, no. 5, pp. 1162–1166 (2015), DOI: 10.1109/TPS.2015.2396081.

[9] Poniaev S.A., Bobashev S.V., Zhukov B.G., Kurakin R.O., Sedov A.I., Izotov S.N., Kulakov S.L., Smirnova M.N., *Small-size railgun of mm-size solid bodies for hypervelocity material testing*, Acta Astronaut, vol. 109, pp. 162–165 (2015), DOI: 10.1016/j.actaastro.2014.11.012.

[10] Hundertmark S., Vincent G., Schubert F., Urban J., *The NGL-60 Railgun*, IEEE Transactions on Plasma Science, vol. 47, no. 7, pp. 3327–3330 (2019), DOI: 10.1109/TPS.2019.2921099.

[11] Siaenen T., Schneider M., Zacharias P., Loffler M.J., *Actively controlling the muzzle velocity of a railgun*, IEEE Transactions on Plasma Science, vol. 41, no. 5, pp. 1514–1519 (2013), DOI: 10.1109/TPS.2013.2245672.

[12] Waindok A., Piekielny P., *Analysis of an iron-core and ironless railguns powered sequentially*, COMPEL – The International Journal for Computation and Mathematics in Electrical and Electronic Engineering, vol. 37, no. 5, pp. 1707–1721 (2018), DOI: 10.1108/COMPEL-12-2017-0533.

[13] Tomczuk B., Koteras D., *Magnetic flux distribution in the amorphous modular transformers*, Journal of Magnetism and Magnetic Materials, vol. 323, no. 12, pp. 1611–1615 (2011), DOI: 10.1016/j.jmmm.2011.01.007.

[14] Wajnert D., Sykulski J.K., Tomczuk B., *An enhanced dynamic simulation model of a hybrid magnetic bearing taking account of the sensor noise*, Sensors, vol. 20, no. 4 (2020), DOI: 10.3390/s20041116.

[15] Wajnert D., *A field-circuit model of the hybrid magnetic bearing*, Archive of Mechanical Engineering, vol. 66, no. 2, pp. 191–208 (2019), DOI: 10.24425/ame.2019.128444.

[16] Vincent G., Hundertmark S., *Using the SR\3-60 railgun in augmented mode*, IEEE Transactions on Plasma Science, vol. 43, no. 5, pp. 1555–1558 (2015), DOI: 10.1109/TPS.2015.2405572.

[17] Jin L., Lei B., Zhang Q., Zhu R., *Electromechanical performance of rails with different cross-sectional shapes in railgun*, IEEE Transactions on Plasma Science, vol. 43, no. 5, pp. 1220–1224 (2015), DOI: 10.1109/TPS.2015.2413892.

[18] Guo X., Dai L., Zhang Q., Lin F., Huang Q., Zhao T., *Influences of Electric Parameters of Pulsed Power Supply on Electromagnetic Railgun System*, IEEE Transactions on Plasma Science, vol. 43, no. 9, pp. 3260–3267 (2015), DOI: 10.1109/TPS.2014.2349997.

[19] Chang X., Yu X., Liu X., Li Z., He H., *A Closed-Loop Velocity Control System for Electromagnetic Railguns*, IEEE Transactions on Plasma Science, vol. 47, no. 5, pp. 2269–2274 (2019), DOI: 10.1109/TPS.2018.2879798.

[20] Liebfried O., Brommer V., *Demonstration of a 1 MJ XRAM Generator Supplying a Medium Caliber Railgun*, IEEE Access, vol. 8, pp. 225018–225031 (2020), DOI: 10.1109/ACCESS.2020.3044441.

[21] Kulkarni A.S., Thomas M.J., *Performance analysis of a self-excited passive compulsator driving a railgun with field winding excited by a secondary armature*, IEEE Transactions on Plasma Science, vol. 47, no. 10, pp. 4738–4744 (2019), DOI: 10.1109/TPS.2019.2939852.

[22] Waindok A., Piekielny P., *Transient analysis of a railgun with permanent magnets support*, Acta Mechanica et Automatica, vol. 11, no. 4, pp. 302–307 (2017), DOI: 10.1515/ama-2017-0046.